RAPID COMMUNICATION

Electrical and thermoelectric study of two-dimensional crystal of $NbSe_2$*

Xin-Qi Li(李新祺)[1], Zhi-Lin Li(李治林)[1], Jia-Ji Zhao(赵嘉佶)[1], and Xiao-Song Wu(吴孝松)[1,2,†]

[1] *State Key Laboratory for Artificial Microstructure and Mesoscopic Physics, Beijing Key Laboratory of Quantum Devices, Peking University, Beijing* 100871, *China*

[2] *Frontiers Science Center for Nano-optoelectronics and Collaborative Innovation Center of Quantum Matter, Beijing* 100871, *China*

(Received 15 March 2020; revised manuscript received 7 May 2020; accepted manuscript online 25 May 2020)

We report experimental investigation of the resistivity and Nernst effect in two-dimensional (2D) $NbSe_2$ crystals. A strongly enhanced Nernst effect, 100 times larger than that in bulk $NbSe_2$, caused by moving vortices is observed in thin film. It is found that in the low temperature, high magnetic field regime, pinning effects show little dependence on the thickness and resistivity of the superconductor films. Strong Nernst signals persist above the superconducting transition, suggesting that the Nernst effect is a sensitive probe to superconducting fluctuations. A magnetic field induced superconductor–insulator transition (SIT) is evident, which is surprising in that such a SIT usually takes place in disordered dirty superconductors, while our samples are highly crystalline and close to the clean limit. Hence, our results expand the scope of SIT into 2D crystal clean superconductors.

Keywords: two-dimensional superconductivity, Nernst effect, superconducting fluctuations, superconductor–insulator transition

PACS: 74.78.−w, 74.25.fg, 74.40.Kb, 74.40.−n **DOI:** 10.1088/1674-1056/ab9614

1. Introduction

More and more highly crystalline two-dimensional (2D) superconductors are emerging, thanks to the development of new fabrication techniques, such as molecular beam epitaxy[1–3] and mechanical exfoliation.[4–6] Earlier studies on 2D superconductivity were usually focused on either quasi-2D systems, e.g., layered high-temperature superconductors, or disordered ultra-thin films, which are in the dirty limit.[7–9] Crystalline 2D superconductors present an idea platform for the investigation of 2D superconductivity in the clean limit and hence have immediately attracted significant interest.[4,6,10–12] New effects, for instance, Ising superconductivity, have been discovered in $NbSe_2$,[4,13] MoS_2,[10,11] WS_2.[14] The so-called quantum Griffiths phase, predicted 40 years ago, has finally been confirmed by experiment in Ga thin films.[15] The elusive Bose metal has been found to appear in crystalline 2D superconductors,[6,16] which poses strong constraints on theoretical models.[17,18] Being readily tuned by gating or surface modification,[12,19,20] this class of materials may provide a great opportunity in understanding the high-temperature superconductivity.[21,22] Currently, the experimental studies have been largely limited to resistance measurements, by which the critical temperature (T_c) and critical field (B_{c2}) are obtained.[23] It is necessary to employ other techniques to gain more insights into 2D superconductivity.

The Nernst effect is the generation of a transverse electric field by a longitudinal thermal gradient in the presence of a magnetic field. In normal metals, this electric field is produced by quasiparticles deflected by Lorentz force. In superconductors, vortex flow driven by a temperature gradient also generates a transverse field, contributing to the Nernst effect. Therefore, it offers information on vortex dynamics and was used in studies of the mixed state of conventional type-II superconductors.[24–26] In high-temperature superconductors, the Nernst effect has proved to be a unique tool in detecting vortex-like excitations in the pseudogap regime above T_c.[27] Recently, it has been used to probe superconducting fluctuations above T_c or B_{c2} in amorphous or granular thin films.[9,28,29] However, to the best of our knowledge, study of the Nernst effect in highly crystalline 2D superconductors has not been reported.

In this work, we carry out measurements of the electrical resistance and the Nernst effect on a 2D crystal superconductor $NbSe_2$. In the thinnest film, 4.5 nm thick, the Nernst signal is strongly enhanced, 100 times larger than that in bulk crystal.[30] The transport entropy of vortices is obtained from the resistance and the Nernst effect. The effect of vortex pinning on the vortex flow is inferred through a phenomenological analysis. It is found that pinning is not affected by reducing the thickness and the number of point defects in the low temperature, high magnetic field regime. Intriguingly, even though our samples are close to the clean limit of a superconductor, a superconductor–insulator transition (SIT) is un-

*Project supported by the National Key Basic Research Program of China (Grant No. 2016YFA0300600) and the National Natural Science Foundation of China (Grant Nos. 11574005 and 11774009).

†Corresponding author. E-mail: xswu@pku.edu.cn

ambiguously identified by scaling of magnetoresistance. The critical component is estimated to be 0.55, smaller than the lower bound of 1 for a disorder dominated SIT, while it is consistent with the clean limit where the interaction dominates.

2. Experiments

The 2*H*-$NbSe_2$ single crystals were grown by chemical vapor transport method. $NbSe_2$ powder (starting material) and iodine (transport agent) were sealed in an evacuated quartz ampoule and then exposed to a temperature gradient from 850 °C to 800 °C for two weeks, forming single crystals at the cooler end. Our bulk crystals have a residual resistivity ratio (RRR) of about 25.6 with $T_c = 7.13$ K, as shown in Fig. 1(c). Thin $NbSe_2$ flakes were exfoliated from the bulk crystals in air and transferred onto Si/SiO_2 substrate. The samples were stored in inert gas environment and only exposed to air during transferring. Fabrication of devices by standard e-beam lithography for transport measurements was completed in 12 hours to reduce oxidation. Measurements of the film thickness were carried out using atomic force microscopy after low temperature transport measurements. An optical image of the setup for measurement of the Nernst effect is shown in Fig. 1(a). Metal stripes made of Ti (5 nm)/Au (50 nm) were used as micro-heaters to generate a temperature gradient across the sample. Usually, stripes of the same metal film deposited with heaters are used as thermometers.[31] However, because the resistance of the gold film saturates below 10 K due to residual resistance, it cannot be used at low temperatures. In this work, we employed disordered graphene stripe as the thermometer, as it can be made to exhibit a strong temperature dependent resistance below 10 K. By patterning an heater of the same geometry as that for measuring a sample and a series of graphene thermometers at different distances to the heater, we estimated the temperature gradient along our samples *ex situ*. An ac method using a lock-in amplifier (SR830 by Stanford Research Systems) at a low frequency of 3.777 Hz was employed. To avoid experimental artifacts due to the strong temperature dependence of the Seebeck coefficient at the superconducting transition,[32] two heaters were used and both were injected with a sinusoidal current of the same frequency but a $\pi/2$ phase difference from an ac current source (Keithley 6221). The amplitude of the currents was adjusted such that the dc temperature gradient between the two transverse Nernst probes was zero. The resistance of the heaters ranges from 12 Ω to 14 Ω. The amplitude of the heating currents (I_H) varies from 230 μA to 290 μA. For the measurement at the lowest temperature, 1.46 K, a heating current of 247 μA was applied, giving rise to a temperature gradient of 50 mK/μm. As shown in Fig. 1(b), the linearity of the Nernst voltage to I_H^2 indicates that the Nernst signal remains linear in temperature gradient. The magnetic field was swept at a rate up to 0.2 T/min.

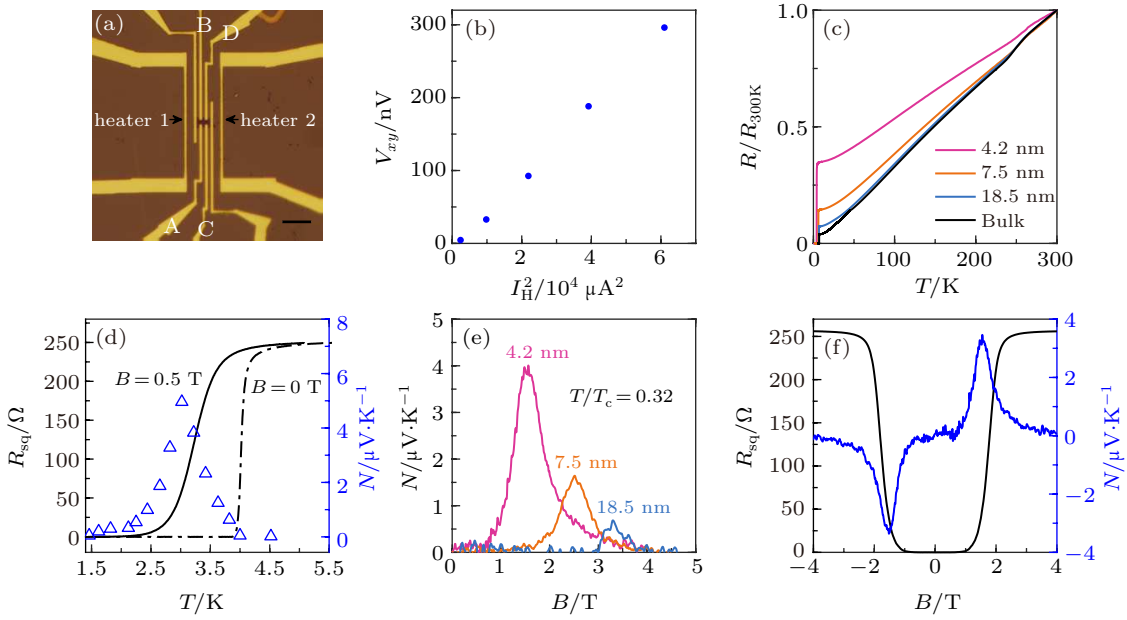

Fig. 1. Strong enhancement of the Nernst effect in 2D $NbSe_2$. (a) Optical image of a device for probing the Nernst signal. A, B and C, D are the Nernst probes. The scale bar is 10 μm. (b) I_H^2 dependence of the Nernst voltage at $T = 1.47$ K and $B = 1.5$ T. (c) Temperature dependence of the normalized resistance for samples with different thicknesses. (d) Temperature dependence of the sheet resistance and Nernst signal for S5 at $B = 0.5$ T. The dash line is the temperature dependence of the sheet resistance at $B = 0$ T. (e) Field dependence of N with different thicknesses at $T/T_c = 0.32$. (f) Field dependence of N and R at $T = 1.4$ K.

3. Results and discussion

The basic information of three samples presented in this study is summarized in Table 1. The RRR of 2.9 in a 4.2 nm thick sample (S5) is similar to that of 2.7 in a 5.5 nm thick sample in previous work.[33] The sheet resistance R_{sq} as a function of temperature in S5 is displayed in Fig. 1(d). The R_{sq}–T curve exhibits a sharp transition at T_c, while above

T_c the resistivity shows a gradual reduction when approaching T_c. The feature above T_c is attributed to superconducting fluctuations, which will be discussed later in detail. T_c is 4.18 K, defined as the temperature at which the resistance is 90% of the normal state value. It is slightly lower than the critical temperature (5.26 K) of a clean bilayer of $NbSe_2$ protected by an insulating layer of hexagonal boron nitride (BN).[6] The suppressed T_c is likely due to oxidation on the surface of the sample. The sheet resistance in the normal state is $R_n = 250\ \Omega$, which is much smaller than the quantum resistance $R_Q = h/4e^2 \approx 6.5\ k\Omega$, indicating that our sample is distinct from highly disordered superconducting amorphous films.[8]

The temperature dependence of the Nernst signal $N = E_y/(-\nabla_x T)$ and sheet resistance at $B = 0.5$ T are plotted in Fig. 1(d). R_{sq} shows a broad transition which is a consequence of dissipation due to vortex motion. N displays a peak at 3 K. It is essentially zero at the normal state or far below T_c. The field dependence of N exhibits a similar peak feature, as seen in Fig. 1(e). We plot the data for two other samples with different thicknesses (S7, 7.5 nm and S9e, 18.5 nm) in the same panel. It is apparent that the Nernst signal is strongly enhanced in the thin flakes. In fact, the peak amplitude of N in the thinnest sample, S5, is 100 times larger than that in bulk $NbSe_2$, about 0.03 μV/K at a magnetic field of 1 T.[30] It is comparable to that in high-temperature superconductors[34] or amorphous superconducting thin film.[28] The peak for the thicker sample shifts towards a higher magnetic field due to its larger upper critical magnetic field. In Fig. 1(f), we plot R_{sq} and N as a function of magnetic field at $T = 1.47$ K. N peaks at 1.55 T, slightly lower than the middle point of the resistance transition.

Table 1. Basic information of samples presented in this study.

Sample	Thickness	ρ_n	Mean free path	Ginzburg–Landau coherence length at 0 K	$\eta/10^{-8}$ N·s·m^{-2} at $T/T_c = 0.32$	T_c	RRR
S5	4.2 nm	110 μΩ·cm	11.7 nm	9.1 nm	0.4	4.18 K	2.9
S7	7.5 nm	7.2 μΩ·cm	106 nm	8.1 nm	9.6	6.13 K	7.0
S9e	18.5 nm	9.3 μΩ·cm	110 nm	–	10.8	6.88 K	13.9

The magnetic field dependence of the Nernst signal at different temperatures in S5 and S7 is shown in Figs. 2(a) and 2(c), respectively. The Nernst peak, occurring at B_p^N, shifts towards a lower field with increasing temperature, as the critical field decreases with temperature. The peak height displays a non-monotonic dependence on temperature, reaching its maximum at $T^*/T_c = 0.69$ in S5 and at $T^*/T_c = 0.68$ in S7. A similar value of $T^*/T_c = 0.57$ was observed in high-temperature superconductors.[35]

Since the Nernst effect in the normal state is negligible, the observed N in the superconducting state can be exclusively attributed to vortex flow. Note that a superconducting vortex carries an excess entropy in its core. Under a thermal gradient $\nabla_x T$, it is subject to a thermal force per unit length of vortex line, $F_{th} = S^*(-\nabla_x T)$, where S^* is the transport entropy per unit length of the vortex line. As a result, a vortex moves toward the low temperature side at a speed of $v_\phi = S^*\nabla_x T/\eta$, determined by the balance between F_{th} and the viscous drag $F_\eta = \eta v_\phi$, where η is the coefficient of viscosity. According to the Josephson relation, this longitudinal flow of vortex generates a transverse field, $E_y = n\phi_0 v_\phi$, where n is the areal density of vortices and ϕ_0 is the superconducting flux quantum. Taking $B = n\phi_0$, one can reach

$$N = \frac{E_y}{\nabla_x T} = \frac{BS^*}{\eta}. \quad (1)$$

Here, η can be inferred from the flux flow resistivity ρ using a similar analysis based on the balance between the force driven by the electric current and the viscous drag

$$\rho = B\phi_0/\eta. \quad (2)$$

Therefore, we can obtain S^* from the measurements of N and ρ, as shown in Figs. 2(b) and 2(d). With increasing field or temperature, the superconductivity is weakened. So, S^* is reduced too. Overall, S^* in S5 is smaller than that in S7, which is reasonable as not only T_c is lower in S5, but the effects of superconducting fluctuations are enhanced by the reduced dimensionality and disorder.[36,37] Despite suppression of the entropy in thin films, the Nernst signal is enhanced, indicating that η is reduced.

The viscosity of vortex results from dissipation by a current through the normal core. Thus, it is related to the normal state resistivity ρ_n and can be expressed as $\eta = \phi_0 B_{c2}/\rho_n$ according to the Bardeen–Stephen theory.[38] As the thickness is reduced, the resistivity increases significantly, leading to reduction of η. According to Eq. (2), the flow resistance should be linear in B, whereas this behavior has not often been seen or at most takes place only in a limited field regime. The reason is that the vortex flow is complicated by pinning and vortex interaction in high fields where the vortex separation is small. To gain a basic, yet meaningful, assessment on how these effects can affect η, we limit our analysis on a simple phenomenological level. One of the effects is that some vortices are trapped by pinning centers. One may adopt a two-fluid model to describe it, i.e., although the total density of vortices is $n = B/\phi_0$, the actually density of vortices that can flow and produce an electric field is $n^* = wB/\phi_0$, where $0 \le w \le 1$, $w = 0$ below the vortex melting field B_m and $w = 1$ at B_{c2}. It is a function of B and T. These trapped vortices distort the flow of other vortices, leading to an increase in η. Additionally, the interaction be-

tween vortices, becoming more important in high fields (small inter-vortex spacing), will also contribute to η. These effects can be included in an enhancement factor of u ($u > 1$) to η. For simplicity, we introduce a new correction term $\chi = u/w - 1$ to account for the pinning and vortex interaction, so that the effective coefficient of viscosity is $\eta^* = (1+\chi)\eta$. It can be readily seen that $\chi = \eta^*/\eta - 1 = \rho_n B/\rho B_{c2} - 1$. The χ is expected to reduce to 0 at B_{c2}, as $\eta = \phi_0 B_{c2}/\rho_n$. Note that the estimation of the entropy S^* is not affected by this new term, as η appears in the expressions for N and ρ and cancels.

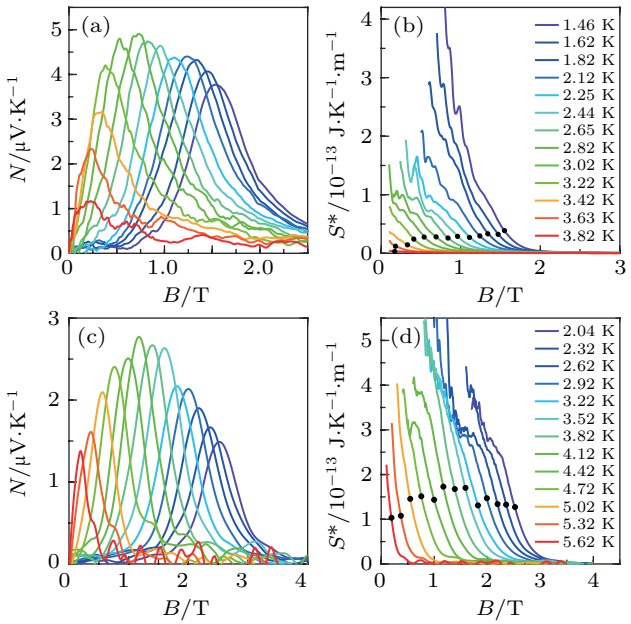

Fig. 2. Field dependence of (a), (c) the Nernst signal and (b), (d) transport entropy carried by vortices in two samples at different temperatures. Black dots denote the entropy at each temperature when the Nernst signal is at its peak.

To see how pinning and vortex interaction change in samples with different thicknesses, we plot χ as a function of reduced magnet field B/B_{c2} at different reduced temperatures for S5 and S7, as shown in Fig. 3. When the temperature is close to T_c, χ in S5 is below that in S7, suggesting that it is easier for vortices to flow in thinner films, even though there are much more defects, as indicated by the sheet resistance. This is because these defects, most likely atomic defects induced by surface oxidation, are much smaller than the coherence length. They are not effective in pinning the vortices, which is consistent with the general belief for disordered amorphous thin films.[39] On the other hand, as the system approaches to the two-dimensional limit, the effect of thermal fluctuations is enhanced, which facilitates vortex flow. With decreasing temperature, this difference reduces. Below $T/T_c = 0.38$, χ in S5 and S7 overlaps at $B/B_{c2} > 0.5$, suggesting that when the thermally-assisted vortex flow is negligible, pinning is not appreciably affected by reducing dimension.

The non-monotonic behavior of the Nernst effect can be understood based on the field and temperature dependence of S^* and η^*. S^* decreases with increasing field due to back-flow of entropy-carrying quasiparticles about the vortex through tunneling.[40] At the same time, η^* decreases too, because not only the pinning energy reduces, but the vortices become more mobile owing to thermally assisted depinning. Two mechanisms compete, in addition to the factor of B, giving rise to a peak feature in N. When the temperature rises, the same argument holds. It is worth pointing out that the entropy should disappear at very low temperature according to the third law of thermodynamics, although we have not seen such a trend, likely because the temperature is not low enough.

From the field dependence of the resistivity, we define the melting field of the vortex lattice B^R_m, upper critical field B^R_{c2}, and the half resistivity point $B^R_{50\%}$. Resultantly, the phase diagrams for S5 and S7 are shown in Fig. 4. We also plot three field scales obtained from the Nernst signal, i.e., the fields at which N appears, peaks, and disappears, denoted as B^N_m, B^N_p, and B^N_{c2}, respectively. In S5, the vortex liquid region is wider than that in S7, which is consistent with the enhancement of fluctuations and penetration depth in 2D. The field scales obtained from N agree well with those from resistivity, except for B^N_{c2}, which is appreciably larger than B^R_{c2} in S5. This can be clearly seen in the experiment raw data shown in Figs. 4(c) and 4(d). In S7, both ρ and N fade at the same field. In contrast, N persists to a higher field than ρ in S5, manifested as a long tail above B^R_{c2}. A Nernst signal surviving well above the upper critical field has been observed in other two-dimensional superconductors. It is believed to result from the short-lived cooper pairs[9,28] or mobile vortices[29,41] in the insulating side of a superconductor–insulator transition.

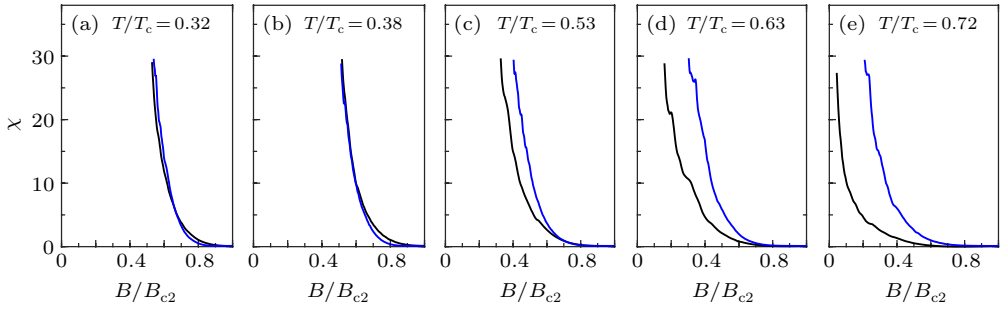

Fig. 3. The χ as a function of reduced magnetic field B/B_{c2} at different reduced temperatures for S5 (black) and S7 (blue). (a) $T/T_c = 0.32$, (b) $T/T_c = 0.38$, (c) $T/T_c = 0.53$, (d) $T/T_c = 0.63$, (e) $T/T_c = 0.72$.

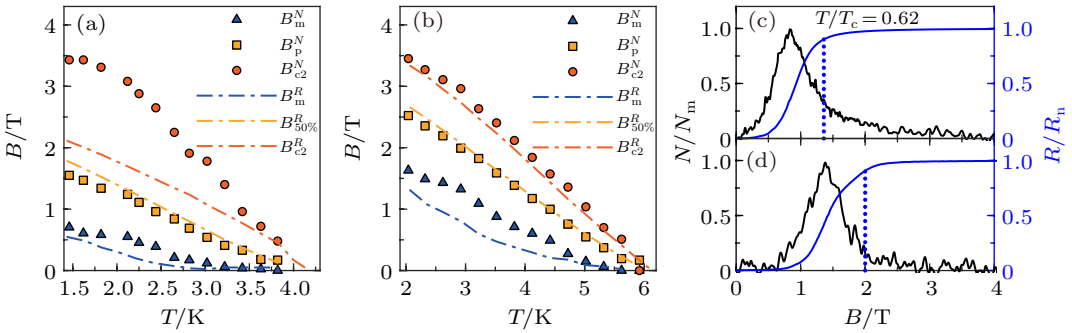

Fig. 4. The B–T phase diagrams. (a), (b) Characteristic fields obtained from the resistance and the Nernst signal for samples S5 and S7, respectively. (c) Field dependence of the normalized Nernst signal and resistance in S5 at $T/T_c = 0.62$, showing a tail above B^R_{c2}. (d) Field dependence of the normalized Nernst signal and resistance in S7 at $T/T_c = 0.62$, showing no tail above B^R_{c2}. The blue dotted line marks B^R_{c2}.

One of the characteristics of a magnetic field induced SIT is a crossing point in the magnetoresistance. Figure 5(a) shows the field dependence of the resistance in S5 measured at various temperatures ranging from 1.43 K to 5.03 K. The zoom-in of the same set of data at the end of the transition is shown in Fig. 5(b). All curves cross at the same point ($B_c = 2.82$ T, $R_c = 253.32$ Ω). This feature can also be illustrated as a temperature independent resistance at $B = 2.8$ T, displayed in the inset of Fig. 5(b). For $B < B_c$, the resistance continues to drop with decreasing temperature, indicating a superconducting phase. For $B > B_c$, the resistance rises with decreasing temperature, indicating an insulating phase. This transition is not driven by temperature but a magnetic field and is a quantum phase transition. Around the transition, the resistance is expected to follow a scaling function

$$R(\delta, T) = R_c f(|B - B_c| T^{-1/z\nu}), \tag{3}$$

where $f(x)$ is the scaling function, z is the dynamic critical exponent, and ν is the correlation length critical exponent. As shown in Fig. 5(c), we plot the ratio R/R_c against the scaling variable $t|B - B_c|$ for 16 different temperatures ranging from 1.43 K to 5.03 K, where $t = (T/T_0)^{-1/z\nu}$. We are able to find the value of $t(T)$ so that all curves collapse onto two branches. By plotting $\ln T/T_0$ as a function of $\ln t$ in Fig. 5(d), we find a good linear relation. From the slope, $z\nu = 0.55$ is obtained. The crossing point and the good agreement of our data with Eq. (3) indicate that there is an SIT in our thinnest film S5. We would like to emphasize that such a SIT is usually found in disordered superconducting films, where the sheet resistance is close to the quantum resistance $h/4e^2$ predicted by theory.[42] Although SIT has been found in films of much lower resistivity in later experiments, the sheet resistance of S5, 250 Ω/sq, is still less than one-half of the lowest resistance ever reported.[43] The observation of SIT in our single crystal film raises an interesting question, i.e., is the transition observed here the same as the one in disordered films, or does the former belong to the same universality class as the latter?

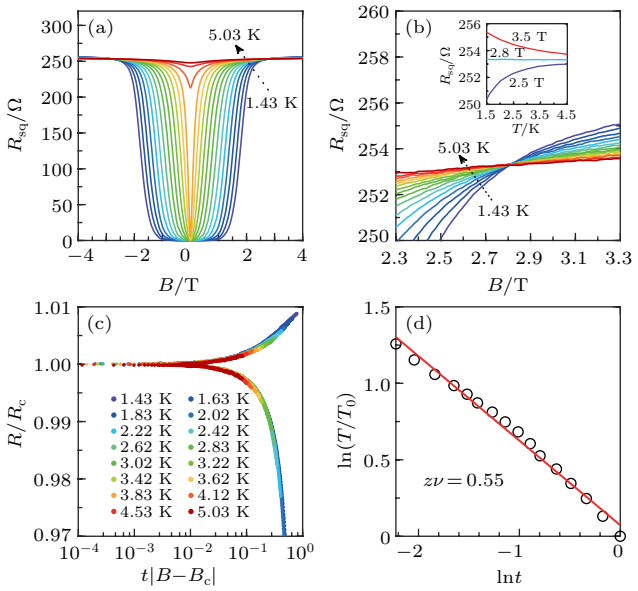

Fig. 5. Magnetic field induced SIT in S5. (a) Magnetoresistance of sample S5 at different temperatures ranging from 1.43 K to 5.03 K. (b) Zoom-in plot of magnetoresistance in (a) near the crossing point. Inset: R_{sq} as a function of temperature at $B = 2.5$ T, 2.8 T, and 3.5 T. (c) Normalized resistance R/R_c as a function of the scaling variable $t|B - B_c|$. (d) $\ln(T/T_0)$ versus $\ln t$. The red line is a linear fit. The $z\nu$ value is obtained from the slope of the fit.

Regarding the question, it would be helpful to discuss the critical exponent ν, which takes different values in different universality classes. Assuming the dynamical exponent $z = 1$, which has usually been found and corresponds to the long-range Coulomb interaction,[42] one has $\nu = 0.55$. In disorder 2D superconductors, it has been predicted that $\nu \geq 1$. Most experiments found so, but there are a few exceptions. Speculations on the nature of disorder have been proposed to account for the discrepancy.[44–46] Very recently, Roy *et al.*[47] have obtained ν from the Nernst effect in amorphous InO_x films and found that the scaling of the transverse Peltier coefficient α_{xy} yields $\nu \sim 0.7$. They argued that α_{xy} is more appropriate for the determination of ν, as it is a thermodynamic property, while the resistance is not. $\nu \sim 0.7$ suggests that their system is in clean limit and dominated by interactions instead of disorder. In terms of relative amplitudes of the mean free path and the coherence length, our samples are close to the limit of clean superconductors and much cleaner than all the other SIT

systems. However, it is not clear if this cleanness can lead to the clean limit in a Josephson coupling islands model, which has been considered to be a relevant model for SIT.

4. Conclusion

We have studied the electric and thermoelectric transport properties of a 2D crystalline superconductor, $NbSe_2$. A strong enhancement of the Nernst effect with decreasing thickness has been observed. In low temperature and high magnetic field, vortex pinning is found to remain unchanged in thinner and more resistive films. Superconducting fluctuations manifest in the Nernst signal much more strongly than in the resistance. Despite being a superconductor close to the clean limit, our thinnest film exhibits a magnetic field induced SIT, evidenced by a scaling behavior in the magnetoresistance. The critical exponent ν is estimated as 0.55, in contrast to $\nu > 1$ in most disordered superconductors.

References

[1] Qin S Y, Kim J, Niu Q and Shih C K 2009 *Science* **324** 1314
[2] Wang Q Y, Li Z, Zhang W H, Zhang Z C, Zhang J S, Li W, Ding H, Ou Y B, Deng P, Chang K, Wen J, Song C L, He K, Jia J F, Ji S H, Wang Y Y, Wang L L, Chen X, Ma X C and Xue Q K 2012 *Chin. Phys. Lett.* **29** 037402
[3] Liao M H, Zang Y Y, Guan Z Y, Li H W, Gong Y, Zhu K J, Hu X P, Zhang D, Xu Y, Wang Y Y, He K, Ma X C, Zhang S C and Xue Q K 2018 *Nat. Phys.* **14** 344
[4] Xi X X, Wang Z F, Zhao W W, Park J H, Law K T, Berger H, Forró L, Shan J and Mak K F 2015 *Nat. Phys.* **12** 139
[5] Gan Y, Cho C W, Li A, Lyu J, Du X, Wen J S and Zhang L Y 2019 *Chin. Phys. B* **28** 117401
[6] Tsen A W, Hunt B, Kim Y D, Yuan Z J, Jia S, Cava R J, Hone J, Kim P, Dean C R and Pasupathy A N 2016 *Nat. Phys.* **12** 208
[7] Shalnikov A 1938 *Nature* **142** 74
[8] Marković N, Christiansen C and Goldman A M 1998 *Phys. Rev. Lett.* **81** 5217
[9] Pourret A, Aubin H, Lesueur J, Marrache-Kikuchi C A, Bergé L, Dumoulin L and Behnia K 2006 *Nat. Phys.* **2** 683
[10] Lu J M, Zheliuk O, Leermakers I, Yuan N F Q, Zeitler U, Law K T and Ye J T 2015 *Science* **350** 1353
[11] Saito Y, Nakamura Y, Bahramy M S, Kohama Y, Ye J T, Kasahara Y, Nakagawa Y, Onga M, Tokunaga M, Nojima T, Yanase Y and Iwasa Y 2016 *Nat. Phys.* **12** 144
[12] Saito Y, Kasahara Y, Ye J T, Iwasa Y and Nojima T 2015 *Science* **350** 409
[13] Xing Y, Zhao K, Shan P, Zheng F P, Zhang Y W, Fu H L, Liu Y, Tian M L, Xi C Y, Liu H W, Feng J, Lin X, Ji S H, Chen X, Xue Q K and Wang J 2017 *Nano Lett.* **17** 6802
[14] Lu J M, Zheliuk O, Chen Q H, Leermakers I, Hussey N E, Zeitler U and Ye J T 2018 *Proc. Natl. Acad. Sci. USA* **115** 3551
[15] Xing Y, Zhang H M, Fu H L, Liu H W, Sun Y, Peng J P, Wang F, Lin X, Ma X C, Xue Q K, Wang J and Xie X C 2015 *Science* **350** 542
[16] Yang C, Liu Y, Wang Y, Feng L, He Q M, Sun J, Tang Y, Wu C C, Xiong J, Zhang W L, Lin X, Yao H, Liu H W, Fernandes G, Xu J, Valles J M, Wang J and Li Y R 2019 *Science* **366** 1505
[17] Phillips P W 2016 *Nat. Phys.* **12** 206
[18] Brink L, Gunn M, José J V, Kosterlitz M and Phua K K 2018 *Topological Phase Transitions and New Developments* (Sigapore: World Scientific) p. 114
[19] Sajadi E, Palomaki T, Fei Z Y, Zhao W J, Bement P, Olsen C, Luescher S, Xu X D, Folk J A and Cobden D H 2018 *Science* **362** 922
[20] Cao Y, Fatemi V, Fang S, Watanabe K, Taniguchi T, Kaxiras E and Jarillo-Herrero P 2018 *Nature* **556** 43
[21] Yu Y J, Ma L G, Cai P, Zhong R D, Ye C, Shen J, Gu G D, Chen X H and Zhang Y B 2019 *Nature* **575** 156
[22] Ding C, Liu C, Zhang Q H, Gong G M, Wang H, Liu X Z, Meng F Q, Yang H H, Wu R, Song C L, Li W, He K, Ma X C, Gu L, Wang L L and Xue Q K 2018 *Acta. Phys. Sin* **67** 207415 (in Chinese)
[23] Costanzo D, Zhang H J, Reddy B A, Berger H and Morpurgo A F 2018 *Nat. Nanotechnol.* **13** 483
[24] Huebener R P and Seher A 1969 *Phys. Rev.* **181** 701
[25] Huebener R P and Seher A 1969 *Phys. Rev.* **181** 710
[26] Rowe V A and Huebener R P 1969 *Phys. Rev.* **185** 666
[27] Xu Z A, Ong N P, Wang Y, Kakeshita T and Uchida S 2000 *Nature* **406** 486
[28] Pourret A, Aubin H, Lesueur J, Marrache-Kikuchi C A, Bergé L, Dumoulin L and Behnia K 2007 *Phys. Rev. B* **76** 214504
[29] Lerer S, Bachar N, Deutscher G and Dagan Y 2014 *Phys. Rev. B* **90** 214521
[30] Bel R, Behnia K and Berger H 2003 *Phys. Rev. Lett.* **91** 066602
[31] Jia Z Z, Li C Z, Li X Q, Shi J R, Liao Z M, Yu, D P and Wu X S 2016 *Nat. Commun.* **7** 13013
[32] Aubin M, Ghamlouch H and Fournier P 1993 *Rev. Sci. Instrum.* **64** 2938
[33] Staley N E, Wu J, Eklund P, Liu Y, Li L J and Xu Z 2009 *Phys. Rev. B* **80** 184505
[34] Wang Y Y, Li L and Ong N P 2006 *Phys. Rev. B* **73** 024510
[35] Wang Y Y, Ong N P, Xu Z A, Kakeshita T, Uchida S, Bonn D A, Liang R and Hardy W N 2002 *Phys. Rev. Lett.* **88** 257003
[36] Skocpol W J and Tinkham M 1975 *Rep. Prog. Phys.* **38** 1049
[37] Pourret A, Spathis P, Aubin H and Behnia K 2009 *New J. Phys.* **11** 055071
[38] Tinkham M 2004 *Introduction to superconductivity*, 2nd Edn. (Courier Corporation) pp. 167–170
[39] Foner S and Schwartz B B 1981 *Superconductor material science: metallurgy, fabrication, and applications,* 1st Edn. (New York: Plenum Press) pp. 735–754
[40] Solomon P R and Otter Jr F A 1967 *Phys. Rev.* **164** 608
[41] Capan C, Behnia K, Hinderer J, Jansen A G M, Lang W, Marcenat C, Marin C and Flouquet J 2002 *Phys. Rev. Lett.* **88** 056601
[42] Fisher M P A 1990 *Phys. Rev. Lett.* **65** 923
[43] Yazdani A and Kapitulnik A 1995 *Phys. Rev. Lett.* **74** 3037
[44] Sørensen E S, Wallin M, Girvin S M and Young A P 1992 *Phys. Rev. Lett.* **69** 828
[45] Cha M C and Girvin S M 1994 *Phys. Rev. B* **49** 9794
[46] Iyer S, Pekker D and Refael G 2012 *Phys. Rev. B* **85** 094202
[47] Roy A, Shimshoni E and Frydman A 2018 *Phys. Rev. Lett.* **121** 047003